

Research on Optimization of Structural Parameters of Plastic-lined Pumps Based on Genetic Algorithm

Xu Fang*, Youmin Wang**, Na Lu*, Qidi Ke* and Binxue Xu*

Keywords: plastic-lined pump, fluid-solid coupling, structural optimization design, genetic algorithm.

ABSTRACT

Low efficiency and small cavitation margin have always been difficult problems for low specific speed pumps. Its impact on plastic-lined pumps is even greater. So in this study, a plastic-lined pump with a specific speed of 65 is used as the research object. PumpLinx was used to simulate the internal flow field of the plastic-lined pump. The internal velocity, pressure, and flow line distribution diagrams were obtained, which verified the reasonability of the overall structure of the model. However, low efficiency and serious cavitation are still problems. The orthogonal test was designed, which uses the impeller inlet diameter, outlet width, vane outlet angle, and vane number as the four factors of the experiment. The efficiency and cavitation were used as evaluation indexes, respectively obtaining the two sets of better structural parameter combinations. Besides, an objective function optimization mathematical model with minimum efficiency loss and cavitation margin of the plastic-lined pump was established. The results of the two sets of orthogonal tests were used as the constraints of the genetic algorithm. The impeller inlet diameter, outlet width, vane outlet angle, and number of vanes were further optimized. The results show that when the impeller inlet diameter is 100mm, the outlet width is 14mm, the vane outlet angle is 27°, and the number of vanes is 6. The efficiency of the plastic-lined pump was increased by 2.36% and the steam volume fraction was reduced by 0.151. The efficiency and cavitation were also significantly improved.

*Paper Received February, 2023. Revised December, 2023.
Accepted January, 2024. Author for Correspondence: Xu Fang*

* Graduate Student, School of Mechanical Engineering, Anhui Polytechnic University, Wuhu, Anhui 241000, China.

** Professor, School of Mechanical Engineering, Anhui Polytechnic University, Wuhu, Anhui 241000, China.

INTRODUCTION

The centrifugal pump has been widely used in various fields because of its features of smooth flow head (HEAD) variation, simple construction, and easy performance adjustment (2015). With the development of the non-ferrous smelting industry, the working environment of centrifugal pumps is becoming more and more complex. Its pumping medium for corrosion resistance also has a higher requirement. Traditional metal pumps are difficult to meet the requirements of corrosion resistance. But plastic-lined pumps have excellent corrosion resistance and high stability and other characteristics, so they are widely used in the chemical industry. With the relevant industries on the performance requirements of the pump constantly improving, it is necessary to make further research on the internal structure and design method of the pump. So that it can improve the efficiency and reliability of the pump while reducing the losses.

Thakkar S (2021) used computational fluid dynamics, response surface methodology, and a multi-objective optimization algorithm. Taking the vane exit angle, vane wrap angle, and vane exit width as design parameters. Meanwhile, they use the multi-objective optimization algorithm to solve the optimal solution between the head and the efficiency of the centrifugal pump. Jaiswal A K (2022) optimized the input power of the centrifugal pump by changing the outlet angle of the impeller blades. By selecting the blade outlet angles of the three meridional sections as design variables, a multi-objective optimization function is designed with the pump shaft power and head as the target, and the multi-objective genetic algorithm is used to find the optimal design parameters. Noon A A (2021) used the design of experiments (DOE) approach. Firstly, 31 different impeller geometries were generated and the results were minimized and maximized using two objective functions of the net positive suction head (NPSHr) and pump efficiency (η) to reduce the cavitation damage and improve the performance of the centrifugal pump. Alawadhi K (2021) used a multi-objective genetic algorithm (MOGA) and response surface methodology (RSM).

Six geometric parameters were used as design variables and pump power, hydraulic efficiency, volumetric efficiency, and pump efficiency were used as objective functions. The method was implemented to design and optimize the structure of a slurry transfer centrifugal pump.

This paper used the velocity coefficient method to complete the design of the structural parameters of the plastic-lined pump according to the performance parameters of the plastic-lined pump. The flow-solid coupling method is used to analyze the structure of the impeller of the plastic-lined pump, which verifies the rationality of the structure of the plastic-lined pump. The pump efficiency and cavitation are used as evaluation indexes, and the structural parameters of the pump are studied using orthogonal tests. The optimization mathematical model is established by using the objective function of minimizing the efficiency loss and cavitation margin of the liner pump, and the optimization is carried out by using a genetic algorithm.

ANALYSIS OF STRUCTURAL DESIGN OF PLASTIC-LINED PUMPS BASED ON FLUID-SOLID COUPLING

The main over-flow components of a pump are the impeller and the worm gear. The performance parameters such as flow rate, head, and efficiency of the pump are related to these structural parameters. The velocity coefficient method is used to design and calculate the structural parameters of the over-flow components of the plastic-lined pump.

Structural design of overcurrent components

The basic parameters of the plastic lined pump design flow $Q=100\text{m}^3/\text{h}$, head $H=80\text{m}$, and rated speed $n=2900\text{rpm}$. using the empirical formula we can calculate the pump inlet diameter $D_s=100\text{mm}$, and outlet diameter $D_d=80\text{mm}$.

According to the overall structural parameters of a plastic-lined pump, the impeller structure of a plastic-lined pump is designed. Impeller inlet diameter $D_j=90\text{mm}$, vane inlet width $b_1=18\text{mm}$, vane outlet width $b_2=10\text{mm}$, impeller outer diameter $D_2=245\text{mm}$. vane inlet placement angle $\beta_1=20^\circ$, outlet placement angle $\beta_2=30^\circ$ are selected. According to the above parameters, the number of blades $Z=6$, thickness $S=6\text{mm}$, and wrap angle $\varphi=110^\circ$. As shown in Figure 1.

According to the impeller structure parameters for plastic-lined pump worm chamber structure design. Base circle diameter $D_3=260\text{mm}$, worm chamber inlet width $b_3=38\text{mm}$, worm casing spacer placement angle $\psi_0=22^\circ$. As shown in Figure 2.

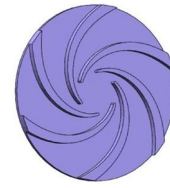


Fig.1. Impeller 3D model drawing



Fig.2. 3D model of worm shell

To avoid excessive influence of the inlet and outlet velocity gradient diffusion on the calculation results, the worm shell outlet is extended appropriately. The three-dimensional model of the plastic-lined pump is shown in Figure 3.

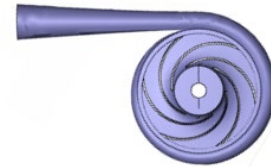


Fig.3. 3D model of plastic-lined pump

Structural analysis of plastic-lined pumps based on fluid-solid coupling

The impeller is the core component of the operation of the plastic-lined pump, and its structural design directly affects the performance of the plastic-lined pump. In this paper, polyethylene is chosen as the material for the impeller of the plastic-lined pump. Polyethylene material is weaker than metal material in terms of wear resistance and pressure resistance. So once the impeller wear problem occurs, the damage is much greater than that of metal pumps. Therefore, in this paper, the flow-solid coupling analysis of the impeller of the plastic-lined pump is carried out by ANSYS to check the rationality of its structural design.

The impeller structure material is polyethylene, and water is selected as the fluid medium. The outlet pressure is set as the outlet boundary condition, and the outlet pressure is 1 atm. the standard turbulence model is selected as the calculation model. The inlet flow velocity of the impeller is set as the inlet boundary condition. The inlet flow velocity of the impeller is calculated to be 3.5m/s. The simulation results are as follows. The inlet and outlet of the impeller, the impeller runner and fluid-solid coupling surface, and the boundary of each wall are all adopted with no-slip wall boundary conditions. In addition, the impeller blades are set to rotating wall conditions. Its rotational speed and direction are the same as the fluid region of the impeller. In the fluid-structure

coupling analysis, the axial displacement constraint is applied to the rear end face of the impeller hub, and the radial displacement constraint and the rotational constraint are added to the inner wall face of the hub.

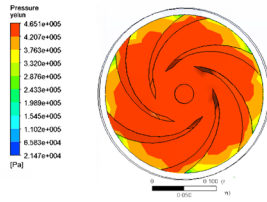


Fig.4. Water pressure distribution diagram

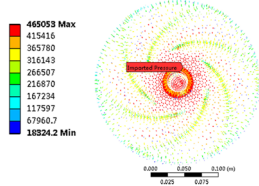


Fig.5. Pressure load loading

As can be seen from Figure 4, the equivalent force under the impeller flow field load is generally distributed axisymmetrically, and there is no obvious sudden change in the pressure distribution in each flow channel. The pressure at the impeller inlet is the largest, and the pressure at the impeller outlet gradually decreases. Impeller in the equal radius blade area, the working surface pressure is generally greater than the pressure in the back area of the blade. From Figure 5 impeller pressure load loading diagram can be seen. The closer the impeller is to the central part, the greater the pressure it has. This part of the pressure comes from the pressure action of the fluid on the impeller surface. The overall distribution of its pressure load corresponds to the water pressure distribution of the flow field in Figure 4.

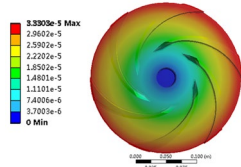


Fig.6. Total impeller displacement deformation diagram

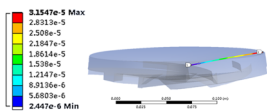


Fig.7. Total deformation deflection curve of impeller

The total deformation of the impeller fluid-solid coupling can be seen in Figure 6. With the increase of impeller radius, the impeller deformation movement also increases gradually. To obtain the deformation displacement at each point of the impeller, deflection curves are established at the center and the edge of the impeller. The center of impeller rotation is marked as point 1, and the edge of the impeller is marked as point 2. Figure 7 shows the total deformation deflection curve of the impeller.

It can be seen in Figure 8. The relative displacement change of point 2 after deformation is $3.1547 \times 10^{-5} \text{m}$. The overall deformation of the impeller is linear from the center to the edge. When the impeller of the plastic-lined pump is made of polyethylene, which is easier to deform, the clearance between the impeller and the pump cover and the inlet width of the vortex chamber are reasonably designed.

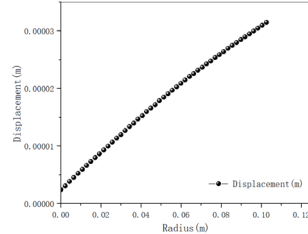


Fig.8. Coordinate diagram of total deflection curve of impeller

NUMERICAL SIMULATION OF THE INTERNAL FLOW FIELD OF THE PLASTIC-LINED PUMP

Boundary condition setting

The impeller and worm gear-related parameters have been obtained in Section 2. Cfturbo software was used to model the impeller and worm housing fluid domains in 3D. The final fluid domain modeling of the overflow components is shown in Figures 9 and 10.

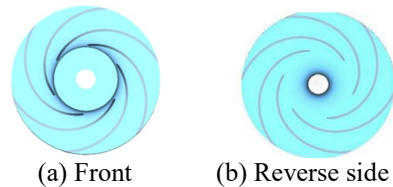


Fig.9. Plastic-lined pump impeller fluid domain three-dimensional modeling



Fig.10. 3D model of worm shell

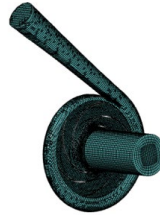


Fig.11. Centrifugal pump meshing

A 3D model of the impeller and worm housing is imported into PumpLinx, and an inlet section is

created at the impeller inlet. Then mesh the inlet section, the impeller, and the worm casing. The mesh is divided as shown in Figure 11.

After completing the mesh division and interaction surface setting for the plastic-lined pump. Set the boundary conditions for speed, flow rate, inlet pressure, etc. As shown in Table 1.

Table 1. Boundary condition parameter settings

Pump Flow Rate	Pump Speed	Head	Fluid Media	Media Density	Turbulence Medium	Atmospheric Pressure	Dynamic Viscosity
m ³ /h	r/min	m	—	kg/m ³	—	Pa	×10 ⁻³ Pa·S
100	2900	80	Water	998.2	Standard k-ε	101325	1.003

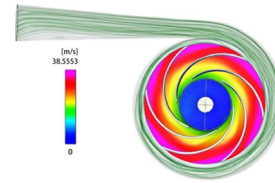


Fig.14. Speed contour of plastic lined pump

Numerical simulation analysis of plastic-lined pumps

Because the impeller tends to have a low-pressure area during operation, it is prone to cavitation. This generates noise and vibration and damages the overflow components. To monitor the area and degree of cavitation occurrence. Both water (liquid) and water (steam) media are selected for multiphase flow simulation. The number of computational iterations set in this paper is 1000 steps, and Figure 12 shows the convergence of the iterative residual curves.

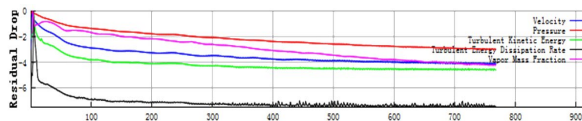


Fig.12. Residual curve graph

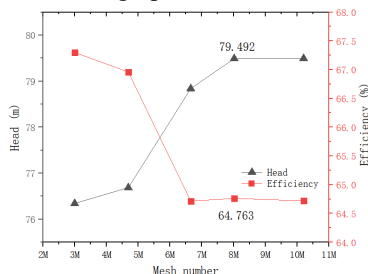


Fig.13. Mesh irrelevance analysis

It can be seen from Figure 13. With the increase of the grid number, the head and efficiency gradually tend to be smooth. Considering the computational resources. To balance the accuracy and efficiency of the calculation, the final grid number is determined as 8021379.

Velocity field analysis

Figure 14 shows the velocity cloud of the plastic-lined pump. The overall fluid velocity inside the impeller of the plastic-lined pump is symmetrical, and the closer to the outer edge of the impeller, the higher the velocity. Impeller in the same radius area, the speed of the blade working surface is less than the speed of the back of the blade. It means that the velocity distribution inside the impeller is reasonable.

Pressure field and cavitation analysis

Figure 15 shows the pressure cloud of the plastic-lined pump. The pressure is lowest in the inlet area of the plastic-lined pump. The closer to the snail casing, the higher the pressure is, and the pressure is highest at the snail casing outlet. The pressure gradually becomes larger from the impeller inlet to the outlet. The overall pressure field inside the impeller is distributed in an axisymmetric pattern. There is no obvious mutation area between the inside of the impeller and the flow path of the worm shell. So the pressure distribution of the plastic-lined pump is reasonable.

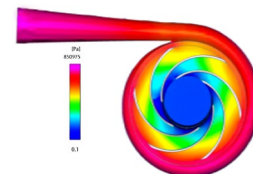


Fig.15. Pressure contour diagram of plastic lined pump

Near the impeller inlet area, the pressure is lowest and the difference between high and low pressure is large. This area is the most prone to cavitation. The appearance of cavitation inside the pump will seriously jeopardize the safe operation of the pump, cause the performance of the pump to decline, generate vibration, damage the overflow components, and shorten the life of the pump. In this paper, the flow field simulation uses the steam mass fraction inside the lined pump to reflect the location of cavitation, and the steam volume fraction to reflect the degree of cavitation. The higher the vapor volume fraction, the more serious the cavitation inside the lined pump.

It can be seen in Figure 16. The steam mass fraction after the liner pump reaches stable convergence is 1.7926×10^{-5} . The cavitation is mainly concentrated in the back area of the blade on the side of the tongue, and there is slight cavitation in the head of the blade. At the same time, combined with the analysis of the impeller pressure cloud in Figure 14 of the liner pump, the prediction of the location of cavitation was verified.

From Figure 17 liner pump steam volume

fraction diagram can be seen. Impeller steam volume fraction of 0.999906. indicates that the pump in this operating condition, the media has reached the critical pressure of vaporization. The medium itself has a certain amount of gas content. So the fluid medium quickly vaporized and produced a large number of steam bubbles. Resulting in a high volume fraction of steam inside the plastic-lined pump, and a more serious cavitation damage.

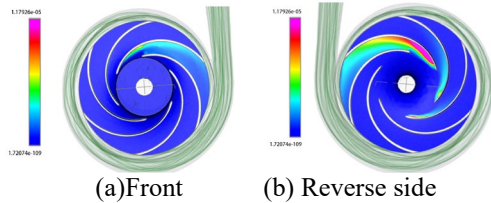


Fig.16. Steam mass fraction for plastic-lined pumps

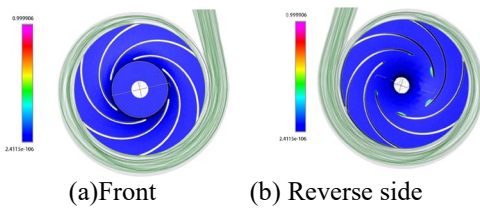


Fig.17. Volume fraction of steam from plastic-lined pump

When the internal flow field of the plastic-lined pump is stable. Its internal velocity, pressure, etc. also tend to be stable values. According to equation 1, the efficiency of the plastic-lined pump can be calculated at this time.

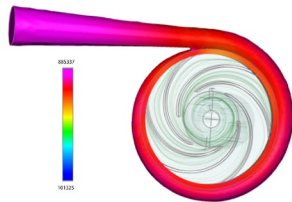


Fig.18. Plastic lined pump outlet pressure diagram

As can be seen from Figure 18. The outlet pressure of the plastic-lined pump is 850975 Pa. The inlet pressure set by the boundary condition is 101325 Pa. The difference between the inlet and outlet pressure is

$$\Delta P = P_{out} - P_{in} = 784012 \text{ (Pa)}$$

According to the pump efficiency calculation formula.

$$H = \frac{\Delta P}{\rho g} \quad (1)$$

$$\eta = \frac{Q}{1000P} \Delta P \quad (2)$$

Where ρ is the density of the fluid medium (kg/m^3), η is the efficiency, P is the shaft power (kW), ΔP is the differential pressure between the pump inlet and outlet.

The calculation yields.

$$\eta = \frac{Q}{1000P} \Delta P = 66.79\%$$

Flow field flow line analysis

After the internal flow field of the liner pump is stabilized, its internal flow field flow line distribution is shown in Figure 19. The flow line distribution between the impeller vanes is uniform, and there is some uneven flow line distribution at the worm shell outlet, but there is no sudden change in the distribution in the rest of the place. Figure 20 shows the enlarged view of the worm shell outlet streamlines. It can be seen from the figure that diffusion occurs at the side of the worm shell outlet port, which is related to the length of the worm shell outlet design.

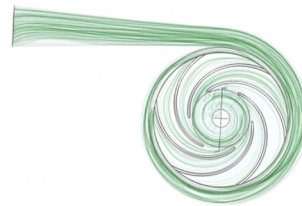


Fig.19. Internal flow diagram of plastic lined pump



Fig.20. Plastic lined pump outlet local flow diagram

The above analysis verifies that the overall structure of this model is reasonable. However, there are problems of low efficiency and serious cavitation. Further optimization of the model structure parameters is needed.

CFD FLOW FIELD ANALYSIS BASED ORTHOGONAL TEST DESIGN

Cavitation has been one of the main factors affecting the efficiency, stability, and life of the pump. The efficiency of the pump is directly related to the cost of products in industrial production. While improving the efficiency of the pump, it is also necessary to ensure the stability of the pump. In this paper, the efficiency and cavitation of plastic-lined pumps are selected as evaluation indexes for orthogonal tests.

CFD flow field simulation orthogonal test design

In this paper, the impeller inlet diameter D_1 , outlet width b_2 , blade outlet angle β_2 , and the number of blades Z are selected as four factors for the orthogonal test. They are denoted by A, B, C, and D, respectively. The orthogonal test of this design was five levels. That is, a four-factor, five-level orthogonal test. The selected evaluation indexes are the efficiency and cavitation performance of the

plastic-lined pump. According to the selection of factors and levels. It is known that this test is a four-factor, five-level test. So the use of $L_{25}(5^4)$ is most appropriate.

The values of each factor of the orthogonal test and its respective level values for each factor are shown in Table 2.

Table 2 Table of factor levels of orthogonal test

Factors	A(mm)	B(mm)	C(°)	D
Level 1	80	6	26°	4
Level 2	86	8	28°	5
Level 3	90	10	30°	6
Level 4	94	12	32°	7
Level 5	98	14	34°	8

The steam volume fraction and outlet pressure were obtained for each group by simulating 25 groups of parameters for the orthogonal test. The efficiency of the corresponding group of plastic-lined pumps was calculated and the resulting factor values were obtained. The final orthogonal test results obtained by calculation are shown in Table 3.

Table 3. Table of orthogonal tests and results

Serial number	A	B	C	D	Efficiency (%)	Cavitation (Vapor volume fraction)
1	80	6	26	4	63.22	0.978067
2	80	8	28	5	64.86	0.973542
3	80	10	30	6	63.78	0.962341
4	80	12	32	7	65.26	0.988031
5	80	14	34	8	64.95	0.960375
6	86	8	28	6	63.22	0.971398
7	86	8	30	7	64.16	0.961674
8	86	10	32	8	65.58	0.967709
9	86	12	34	4	62.54	0.959413
10	86	14	26	5	64.36	0.980602
11	90	6	30	8	62.11	0.991571
12	90	8	32	4	62.55	0.980605
13	90	10	34	5	63.47	0.961259
14	90	12	26	6	65.29	0.955471
15	90	14	28	7	67.34	0.971307
16	94	6	32	5	68.17	0.963179
17	94	8	34	6	63.35	0.988036
18	94	10	26	7	66.79	0.973451
19	94	12	28	8	65.31	0.969079
20	94	14	30	4	62.96	0.960571
21	98	6	34	7	66.28	0.964084
22	98	8	26	8	64.05	0.977471
23	98	10	28	4	63.16	0.979361
24	98	12	30	5	65.03	0.965464
25	98	14	32	6	69.21	0.955461

Analysis of orthogonal test results

The results of the orthogonal tests were processed using the analysis of extreme differences. The results were analyzed by putting efficiency and cavitation as evaluation indexes.

Plastic-lined pump efficiency evaluation analysis

The magnitude of the effect of each process parameter on the efficiency as an evaluation index was calculated using the extreme difference analysis. The results of the analysis are shown in Table 4.

Table 4. Plastic lined pump efficiency extreme difference analysis table

	A	B	C	D
K1	322.07	323	323.71	314.43
K2	319.86	318.97	323.89	325.89
K3	320.76	322.78	318.04	324.85
K4	326.58	323.43	330.77	329.83
K5	327.73	328.82	320.59	322
k1	64.414	64.6	64.742	62.886
k2	63.972	63.794	64.778	65.178
k3	64.152	64.556	63.608	65.966
k4	65.316	64.686	66.154	64.97
k5	65.546	65.764	64.118	64.4
R	1.132	1.078	0.036	1.514

The magnitude of the value of R_m reflects the degree of influence of the factor on the test evaluation indexes. the larger the value of R_m , the greater the influence of the factor on the test evaluation indexes, and vice versa, the smaller the degree of influence. It can be seen from Table 4 according to the value of R_m . The order of influence of each test factor on the efficiency of the evaluation index is $D > A > B > C$ (number of blades > impeller inlet diameter > export width > Blade exit angle). The trend of the influence of each factor on the efficiency is shown in Figure 21.

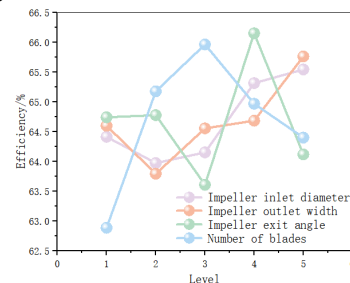


Fig.21. Trend graph of the effect of factors on efficiency

According to the highest efficiency evaluation index, the best combination of structural parameters of the plastic-lined pump can be obtained as $A_5B_5C_4D_3$. The maximum efficiency value can be obtained when the impeller inlet diameter $D_j=98\text{mm}$,

outlet width $b_2=14\text{mm}$, vane outlet angle $\beta_2=32^\circ$, and vane number $Z=6$. The efficiency is 69.21%, which is 2.42% higher than the original model. The test results are shown in Figure 22 and Figure 23.

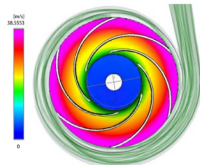


Fig.22. Velocity contour for the combination of $A_5B_5C_4D_3$

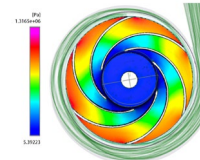


Fig.23. Pressure contour diagram for the combination of $A_5B_5C_4D_3$

Plastic lined pump cavitation evaluation analysis

The cavitation evaluation analysis was performed using the vapor volume fraction as the evaluation index. The results of the analysis are shown in Table 5.

Table 5. Plastic lined pump cavitation situation extreme difference analysis table

	A	B	C	D
K1	4.862356	4.868299	4.865062	4.858017
K2	4.840796	4.870127	4.864687	4.844046
K3	4.860213	4.844121	4.841621	4.832707
K4	4.854316	4.837458	4.854985	4.858547
K5	4.841841	4.828316	4.833167	4.866205
k1	0.9724712	0.9736598	0.9730124	0.9716034
k2	0.9681592	0.9740254	0.9729374	0.9688092
k3	0.9720426	0.9688242	0.9683242	0.9665414
k4	0.9708632	0.9674916	0.970997	0.9717094
k5	0.9683682	0.9656632	0.9666334	0.973241
R	0.004312	0.0083622	0.006379	0.0066996

It is known from Table 5. According to the evaluation index of minimum cavitation damage (minimum steam volume fraction), the best combination of structural parameters of a plastic-lined pump can be obtained as $A_1B_2C_1D_4$. When the impeller inlet diameter D_j is 80mm, outlet width $b_2=8\text{mm}$, vane outlet angle $\beta_2=26^\circ$, and vane number $Z=7$. The steam volume fraction is the smallest, and the cavitation damage is the smallest.

It can be seen from Table 5. According to the evaluation index of minimum cavitation damage (minimum steam volume fraction), the best combination of structural parameters of the plastic-lined pump can be obtained as $A_1B_2C_1D_4$. When the impeller inlet diameter D_j is 80mm, outlet width $b_2=8\text{mm}$, vane outlet angle $\beta_2=26^\circ$, and the number of vane $Z=7$, the steam volume fraction is

minimum, i.e., minimum cavitation damage.

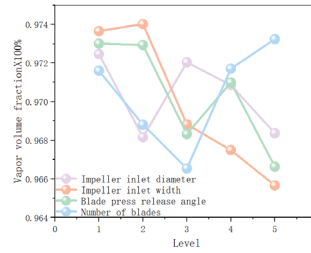


Fig.24. Trend of the influence of various factors on cavitation

The order of influence of each parameter on the efficiency is obtained according to the extreme difference value R: $B>D>C>A$ (inlet width>several blades>blade exit angle>inlet diameter). The trend of the influence of each factor on cavitation is shown in Figure 24.

According to the evaluation index of minimal cavitation damage, the best combination of parameters was obtained as $A_1B_2C_1D_4$ (inlet diameter $D_j=80\text{mm}$, outlet width $b_2=8\text{mm}$, blade outlet angle $\beta_2=26^\circ$, and several blades $Z=7$). The impeller and worm housing were modeled using CFturbo, and PumpLinx was used to divide the mesh to simulate the test, as shown in Figure 25 and Figure 26. The results of the experimental simulation of a steam mass fraction are shown in Figure 27 and Figure 28. The steam volume fraction is 0.90108, and there is a significant decrease in steam volume and a reduction in cavitation damage.

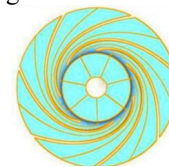


Fig.25. 3D view of the new impeller



Fig.26. New snail shell 3D drawing

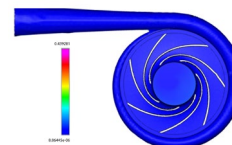


Fig.27. Vapor mass fraction for the combination of $A_1B_2C_1D_4$

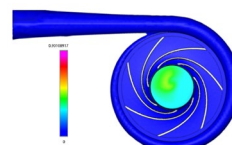


Fig.28. Vapor volume fraction for the combination of $A_1B_2C_1D_4$

MULTI-OBJECTIVE OPTIMIZATION BASED ON GENETIC ALGORITHM

To obtain the combination of structural parameters for the optimal overall performance of the plastic-lined pump. A genetic algorithm is used to take further optimization of the structural parameters of the plastic-lined pump. From the efficiency and life of the plastic-lined pump, each sub-objective function is established separately. The integration objective function method is used to unify each sub-objective function to obtain the unified objective function. The results of the orthogonal test efficiency analysis and cavitation analysis were used as constraints.

Establishment of sub-objective function

Establishment of the minimum efficiency loss objective function

The theoretical head of the pump according to the Stodola formula of reference is

$$H_T = \frac{1}{g}(\mu_2 v_{\mu 2} - \mu_1 v_{\mu 1}) \quad (3)$$

Where H_T is the theoretical head of the pump (m), μ_2 is the vane outlet circumferential velocity (m/s), $v_{\mu 2}$ is the vane outlet absolute velocity circumferential fractional velocity (m/s), μ_1 is the blade inlet circumferential velocity (m/s), $v_{\mu 1}$ is the blade inlet absolute velocity circumferential fractional velocity (m/s).

Assuming no pre-spin at the inlet, the equation $v_{\mu 1} = 0$. According to Stodola's formula

$$H_T = \frac{1}{g} \left[\sigma \left(\frac{\pi n D_2}{60} \right) - \frac{n Q_t}{60 \phi^2 \tan \beta_2} \right] \quad (4)$$

Where ϕ_2 is the impeller outlet discharge coefficient, σ is the Stodola slip coefficient, $\sigma = 1 - \pi/2 \sin \beta_2$, D_2 is the outer diameter of the impeller (mm), n is the rotational speed (m/s).

From equation 4, then

$$D_2^2 = \frac{(g H_T + \frac{n Q_t}{60 \phi^2 \phi_2 \tan \beta_2})}{(1 - \frac{\pi \sin \beta_2}{Z})(\frac{n \pi}{60})^2} \quad (5)$$

According to the impeller exit velocity triangle it is known that

$$v_2^2 = v_{m2}^2 + v_{u2}^2 \quad (6)$$

$$\text{Where } v_{m2} = \frac{Q_t}{\pi D_2 b_2 \phi_2}, \quad v_{u2} = \frac{g H_T}{u_2}$$

From equation (6), then

$$v_2^2 = \frac{1}{D_2^2} \left(\frac{60 g H_T}{n \pi} \right)^2 \left[1 + \left(\frac{n Q_t}{60 g H_T b_2 \phi_2} \right)^2 \right] \quad (7)$$

The energy loss of a centrifugal pump mainly includes volume loss, mechanical loss, and hydraulic

loss. The mechanical loss of the centrifugal pump mainly includes bearing and packing loss P_z and disc friction loss ΔP_d . For low and medium-speed centrifugal pumps, the loss is mainly disc friction loss ΔP_d , and bearing and packing loss P_z can be neglected. The disc loss ΔP_d is calculated by the following formula

$$\Delta P_d = 1.1 \times 75 \times 10^{-6} k \rho g \mu_2^3 D_2^2 \quad (8)$$

Where k is the correction factor, μ_2 is the impeller outlet circumferential velocity (m/s).

As μ_2 contains impeller outer diameter D_2 , it can be seen from equation (8) that the disc friction loss is proportional to the fifth power of impeller outer diameter D_2 . To reduce the disc friction loss, it is necessary to reduce the impeller outer diameter D_2 . As can be seen from Equation 7, the impeller outer diameter D_2 reduction will certainly cause an increase in the exit velocity v_2 , and then cause the worm casing hydraulic loss increases. Simply reducing the friction loss of the disc may increase the total loss of the centrifugal pump, which is not conducive to the improvement of efficiency. Therefore, a comprehensive optimization of the centrifugal pump is needed to achieve optimal performance.

In the efficiency losses of centrifugal pumps. The proportion of the volume loss is small, and the hydraulic and mechanical losses inside the impeller remain the same. Therefore, in this paper, the minimal value of the sum of the friction loss of the impeller disc and the hydraulic loss in the piezometric chamber will be used as the target to establish the optimized mathematical model. According to the formula recommended by literature for calculating the total power loss of centrifugal pumps:

$$\Delta N = \Delta N_h + \Delta N_p = \frac{k_1 \rho Q v_2^2}{2} + k_2 0.35 \times 10^{-2} \rho \omega^3 R_2^5 \quad (9)$$

Where ΔN_h is the hydrodynamic power loss, ΔN_p is the disc friction loss efficiency, k_1 is the coefficient of velocity energy loss within the piezometric chamber, $k_1 = 0.15 \sim 0.25$, k_2 is the dimensionless disc friction coefficient, $k_2 = 0.8 \sim 1.0$, R_2 is the impeller outer edge radius (mm).

Substituting Eqs. 5 and 7 into Eq. 9 yields

$$\Delta N = \frac{K_1 \rho Q}{2} \left[g_2 H_T^2 + \left(\frac{N Q_t}{60 b_2 \phi_2} \right)^2 \right] \left(1 - \frac{\pi \sin \beta_2}{Z} \right) + 0.35 \times 10^{-2} K_2 \rho \left(\frac{30}{n \pi} \right)^2 \left[\frac{g H_T + \frac{n Q_t}{60 b_2 \phi_2}}{1 - \frac{\pi \sin \beta_2}{Z}} \right]^2 \quad (10)$$

The smaller the total power loss is, the more it meets the requirement, i.e. the loss is minimized. So the optimization objective function for maximum efficiency is:

$$\min [f_1(x) = \Delta N_{\min}] \quad (11)$$

The establishment of the minimum cavitation margin objective function

When the pressure of the liquid increases and exceeds the gasification pressure of the bubble, the bubble will re-condense to produce a cavity. At this point, the liquid around the cavity will quickly fill the vacancy. In this part of the vacancy will collide with each other, and the local pressure will rise instantly. The pressure and speed of the liquid in the pump will also change as a result. This will seriously affect the normal operation of the pump, making it produce noise and vibration, reduce efficiency, corrosion of overflow components, and damage the stability of the pump. The impeller of the centrifugal pump will also cause damage to the vane wall surface due to cavitation, which affects the impeller's life.

The basic equation for the pump cavitation margin is

$$NPSHr = \frac{v_0^2}{2g} + \lambda \frac{\omega_0^2}{2g} \quad (12)$$

Set the inlet without pre-spin, then.

$$\begin{cases} v_{u0} = 0 \\ \omega_0^2 = v_0^2 + \mu_0^2 \\ v_0 = k_2 \frac{4Q}{(D_1^2 - d_h^2)\pi\eta_v} \\ \mu_0 = k_1 \frac{\pi n D_j}{60} \end{cases} \quad (13)$$

Where $k_1 = 0.876$, $k_2 = 0.91$.

Substituting equation (13) into equation (12) yields

$$NPSHr = \frac{1}{2g} (1 + \lambda) \frac{k_2^2 4_2^2 Q^2}{(D_1^2 - d_h^2)\pi^2 \eta_v^2} + \lambda \frac{k_1^2 \pi^2 n^2 D_j^2}{2g 60^2} \quad (14)$$

In most cases, $d_h = 0$, the cavitation allowance is

$$NPSHr = \frac{1}{2g} (1 + \lambda) \frac{k_2^2 4_2^2 Q^2}{D_1^4 \pi^2 \eta_v^2} + \lambda \frac{k_1^2 \pi^2 n^2 D_0^2}{2g 60^2} \quad (15)$$

So the minimum objective function of the cavitation margin is

$$\min [f_2(x) = NPSHr] \quad (16)$$

Handling of Objective Functions and Constraints

Currently, multi-objective optimization problems have been widely used in optimization problems in mechanical engineering and other areas. The integrated objective function method solves the limitations of single-objective optimization methods. For a multi-objective optimization problem, the mathematical model can be generally expressed as:

$$\begin{cases} \min F(x) \quad x \in R^n \\ \text{s.t. } g_u(x) \leq 0 \quad u = 1, 2, 3, \dots, m \\ h_v(x) = 0 \quad v = 1, 2, 3, \dots, n \end{cases} \quad (17)$$

Where $F(x) = [f_1(x), f_2(x), \dots, f_n(x)]^T$, $f_n(x)$ is the sub-objective function of $F(x)$.

In this paper, the weight coefficient transformation method is used to deal with multi-objective functions. For a multi-objective optimization problem. According to the different degrees of influence of each sub-objective function on the optimization direction, each sub-objective function $f_i(x)$ ($i=1, 2, \dots, n$) is given the corresponding weight w_i . then the total objective function is

$$\min f(x) = \min \sum_{i=1}^3 w_i \frac{f_i(x) - f_i^*}{f_i^0} \quad (18)$$

Where w_i is the corresponding sub-objective function, f_i^* is the optimal value of the sub-objective function.

Optimization with D_j , b_2 , β_2 , and Z as design variables yields.

$$X = [x_1 \ x_2 \ x_3 \ x_4]^T = [D_j \ b_2 \ \beta_2 \ Z]^T \quad (19)$$

s.t. $x \in X$, $X \in R_m$ denotes the constraint set of the optimization model.

Specific implementation of the algorithm

Parameter setting and chromosome coding

According to the results of several times of algorithm debugging, the final population size is set to 80 chromosomes and the maximum number of iterations is set to 300 generations. Due to the large range of variation of the model parameters to be identified, a floating-point coding is adopted. Each chromosome is represented by a four-dimensional vector:

$$X_i = [X_{i1} \ X_{i2} \ X_{i3} \ X_{i4}]^T$$

where i is the number of the corresponding chromosome in the vector. The four coordinates x_{i1} to x_{i4} of the vector are the codes of the i -th chromosome, which correspond to the parameters D_j , b_2 , β_2 , and Z in the objective function, respectively.

The range of values of the design variables can have an important impact on the optimization results. Both too-narrow and too-wide design ranges of the variables do not yield an effective optimal solution. The constraints of chromosome coding are based on the existing excellent centrifugal pump hydraulic model with the empirical values of the relevant parameters calculated by Equation (20). Take the orthogonal test efficiency and cavitation analysis results as reference values, and appropriately expand their taking margins. Thus, the upper and lower limits of the four coordinates in the chromosome code are determined, as shown in Table 6.

$$\left\{ \begin{array}{l} 3.5\sqrt[3]{\frac{Q}{n}} < D_1 < 4\sqrt[3]{\frac{Q}{n}} \\ 0.6\left(\frac{n_s}{100}\right)^{\frac{5}{6}}\sqrt[3]{\frac{Q}{n}} < b_2 < 0.8\left(\frac{n_s}{100}\right)^{\frac{5}{6}}\sqrt[3]{\frac{Q}{n}} \\ 20^\circ < \beta_2 < 40^\circ \\ 4 < Z < 9 \\ D_j = 0.93D_1 \end{array} \right. \quad (20)$$

Table 6. Range of values for each component of chromosome coding

	Dj	b2	β2	Z
Upper limit value	75	7	25	5
Lower limit value	105	15	33	8

According to the above encoding method, the four components of the vector corresponding to the optimal chromosome output by the genetic algorithm are the model parameter identification results.

Selection operation

Set the probability of selection for each chromosome in the population according to its fitness. The higher the fitness, the higher the probability that the chromosome will be selected into the next generation population. The selection probability is set using a ranking-based selection probability method, in which all chromosomes in the population are ranked from highest to lowest fitness, and the selection probability is set according to this order. The selection probability is calculated by the formula:

$$W_i = e(1 - e)^{i-1} \quad (21)$$

$$p_i = W_i / \sum_{K=1}^N W_k \quad (22)$$

Where W_i is the selection weight of the i -th chromosome in the row, p_i is the selection probability of the chromosome in the row, N is the number of chromosomes in the population, e is the selection weight of the 1st chromosome in the row, and its value ranges from (0,1) to 0.04 in this algorithm.

Crossover operations

Chromosomes to be crossed for the crossover operation are selected randomly based on the crossover probability and paired two by two. The crossover operation is then performed to generate new chromosomes. The crossover probability p_c is set to 0.55. Since the chromosomes are encoded in floating point numbers. Therefore, the crossover operation is implemented using the arithmetic crossover operator. The formula for the arithmetic crossover operation is:

$$\left\{ \begin{array}{l} x_i' = x_i + a(x_{i+1} - x_i) \\ x_{i+1}' = x_{i+1} + a(x_i - x_{i+1}) \end{array} \right. \quad (23)$$

x_i' and x_{i+1}' are the new chromosomes obtained after crossover; a is a random number that takes values in the range (0, 1). The new chromosome generated in the crossover operation can serve to expand the search range of the genetic algorithm and improve the global search capability of the algorithm.

Variational operations

The chromosome to be mutated is randomly selected according to the mutation probability. A new chromosome is generated by randomly selecting one of the four components of its encoding for the mutation operation. The variation probability p_m is set to 0.45. Since the range of values of the components of the chromosome encoding is determined in the constraint, the variation operation is performed using the Gaussian variation operator. The component of the encoding that undergoes variation is replaced by a random variable R . This random variable serves from a Gaussian distribution with expected value μ and standard deviation σ , denoted as :

$$R \sim N(\mu, \sigma^2) \quad (24)$$

Among them:

$$\mu = \frac{X_{\min}^j + X_{\max}^j}{2}, \quad \sigma = \frac{X_{\max}^j - X_{\min}^j}{6}$$

X_{\min}^j and X_{\max}^j are the lower and upper limits of the values of the j th component of the code, respectively. $\mu - 3\sigma = X_{\min}^j$ and $\mu + 3\sigma = X_{\max}^j$, and according to the probability density function of Gaussian distribution, it is known that the probability of the random variable R falling into the $(\mu - 3\sigma, \mu + 3\sigma)$ interval is 99.74%. Therefore the chromosome coding after mutation is still within the range of values limited in the constraint.

Model parameter identification results

After the above steps and 300 iterations, the optimal solution for the parameters of the genetic algorithm recognition model is finally obtained. The evolutionary curve of the optimal fitness with the number of generations n is shown in Fig. 29.

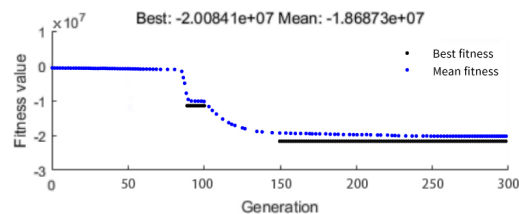


Fig.29. Evolutionary curve of optimal fitness of the population

The final optimization results are shown in Table 7.

Table 7. Parameter optimization results

Parameters	D_j	b_2	β_2	Z
After optimization	99.665	14.011	26.832	5.988
round and rectify	100	14	27	6

Simulation Validation

The plastic-lined pump was modeled again in 3D using the optimized parameters. As shown in Figure 30:

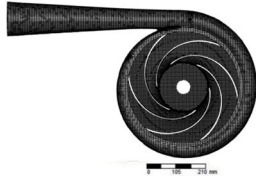


Fig.30. Impeller 3D modeling drawing

Flow field analysis is performed for the newly constructed model guide. It can be obtained from Figure 31. The outlet pressure of the plastic-lined pump is 885337 Pa. The efficiency of the pump can be calculated from the differential pressure between the inlet and outlet of the pump as 71.57%, which is 2.36% higher than the orthogonal test optimization result (69.21%). It can be seen from the steam volume fraction in Figure 32. The steam volume fraction decreased from 0.90108 to 0.750199 before, and the steam volume fraction decreased significantly. The overall performance of the plastic-lined pump was improved.

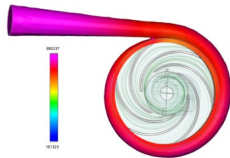


Fig.31. Plastic lined pump outlet pressure

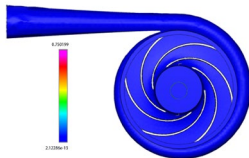


Fig.32. Vapor volume fraction

CONCLUSION

According to the performance parameters required by the plastic-lined pump, the structural parameters of the plastic-lined pump were designed by using the velocity coefficient method, and the structural analysis of the impeller of the plastic-lined pump was carried out by using ANSYS software, which was based on the fluid-solid coupling method to verify the reasonableness of using polyethylene as the material for making the impeller.

PumpLinx was used to simulate the internal

flow field of the plastic-lined pump. By analyzing the velocity field, pressure field, cavitation, efficiency, flow field, and flow line, it is concluded that the overall structure of the liner pump model is reasonable. However, there are problems of low efficiency and serious cavitation.

In this paper, the impeller inlet diameter D_j , outlet width b_2 , vane outlet angle β_2 , and vane number Z are used as four factors in the orthogonal test. The efficiency and cavitation of the plastic-lined pump are selected as the evaluation indexes of the orthogonal test. The best combination of structural parameters $A_5B_5C_4D_3$ for the plastic-lined pump when efficiency is used as the evaluation index has a maximum efficiency of 69.21%, which is 2.42% higher than the original model. When cavitation (vapor volume fraction) is used as an evaluation index, the best combination of structural parameters for the plastic-lined pump is $A_1B_2C_1D_4$, with a vapor volume fraction of 0.90108 and minimal cavitation damage.

To obtain the combination of structural parameters with the optimal comprehensive performance of the plastic-lined pump. A genetic algorithm is used to take further optimization of the structural parameters of the plastic-lined pump. The results of the orthogonal test efficiency analysis and cavitation analysis are used as constraints. The results of structural parameter optimization are $D_j=100\text{mm}$, $b_2=14\text{mm}$, $\beta_2=27^\circ$, and $Z=6$. After flow field analysis. The efficiency of the pump is 71.57%, which is 2.36% higher than the orthogonal test optimization result (69.21%). The vapor volume fraction decreased significantly from 0.90108 to 0.750199 previously. The cavitation problem was significantly improved, and the overall performance of the plastic-lined pump was improved.

AUTHOR CONTRIBUTIONS

Xu Fang had made substantial contributions to design, experimental research, data collection and result analysis; Youmin Wang made critical changes to important academic content; Na Lu, Qidi Ke and Binxue Xu made the final review and finalization of the articles to be published.

DATA AVAILABILITY

The data used to support the findings of this study are included within the article.

CONFLICTS OF INTEREST

The authors declare that they have no conflicts of interest to report regarding the present study.

REFERENCES

Andrew Robison, Andrea Vacca. "Multi-objective

- optimization of circular-toothed gerotors for kinematics and wear by genetic algorithm” [J]. Mechanism and Machine Theory. 2018 (128): 150-168.
- A.P. Masoumi, A.R. Tavakolpour-Saleh. “Experimental assessment of damping and heat transfer coefficients in an active free piston Stirling engine using genetic algorithm” [J]. Energy, 2020 (195):117064.
- Ashutosh.B.Deshmukh, Aditya.A.Lotake, Hrshikesh.N.Paricharak, et al. “Comparative CFD Analysis of Mini Impeller Using Different Materials” [J]. Materials Today: Proceedings ,2020 (24): 2115-2122.
- Guan Shengfan. “Handbook of modern pump technology” [M]. Beijing: Aerospace Press. 1995.
- George Dogkas, Emmanouil Rogdakakis, Panagiotis Bitsikas. “3D CFD simulation of a Vuilleumier heat pump” [J]. Applied Thermal Engineering, 2019 (153): 604-619.
- Gao Z, Liu J, Guo C, et al. “The Strength Study of Thermal Power Unit Absorption Tower Desulphurization Pump Impeller Based on Fluid-Structure Interaction Calculation” [J]. Proceedings of the 15th International Conference on Man–Machine–Environment System Engineering. 2015.
- Hanfei Chen, Peter Hofbauer, Jon P. Longtin. “Multi-objective optimization of a free-piston Vuilleumier heat pump using a genetic algorithm” [J]. Applied Thermal Engineering, 2020 (167):114767.
- Jaiswal A K, Siddique M H, Paul A R, et al. “Surrogate-based design optimization of a centrifugal pump impeller” [J]. Engineering Optimization, 2022, 54(8): 1395-1412.
- K. Vinther, Rene J. Nielsen, Palle Andersen, et al. “Optimization of interconnected absorption cycle heat pumps with micro-genetic algorithms” [J]. Journal of Process Control. 2017 (53): 26-36.
- Liang Quanwei, Wang Zhengwei. “Analysis of static strength and vibration characteristics of mixed-flow rotor” [J]. Journal of Tsinghua University (Natural Science Edition), 2003, 43(12): 1649-1652.
- M. Lorusso, T. Capurso, M. Torresi, et al. “Efficient CFD evaluation of the NPSH for centrifugal pumps” [J]. Nuclear Engineering and Design, 2017 (126): 778-785.
- Marcel Ilie. “Fluid-structure interaction in turbulent flows; a CFD based aeroelastic algorithm using LES” [J]. Applied Mathematics and Computation, 2019 (342): 309–321.
- M. Specklin, P. Dubois, A. Albadawi, et al. “A full immersed boundary solution coupled to a Lattice–Boltzmann solver for multiple fluid–structure interactions in turbulent rotating flows” [J]. Journal of Fluids and Structures. 2019 (90): 205-229.
- Nicola Aldi, Carlo Buratto, Michele Pinelli, et al. “CFD Analysis of a non-Newtonian fluids processing pump” [J]. Energy Procedia, 2016 (101): 742-749.
- Peng-Nan Sun , David Le Touz’e , Guillaume Oger, et al. “An accurate FSI-SPH modeling of challenging fluid-structure interaction problems in two and three dimensions” [J]. Ocean Engineering, 2021 (221): 108552.
- R.Ramirez, E. Avila, L. Lopez, et al. “CFD characterization and optimization of the cavitation phenomenon in dredging centrifugal pumps” [J]. Alexandria Engineering Journal, 2020 (59): 291-309.
- S.Kelbij Star, Giuseppe Spina, Francesco Belloni, et al. “SDevelopment of a coupling between a system thermal–hydraulic code and a reduced order CFD model” [J]. Annals of Nuclear Energy, 2021 (153): 108056.
- Sreevatsa Anantharamu, Krishnan Mahesh . “Response of a plate in turbulent channel flow: Analysis of fluid–solid coupling” [J]. Journal of Fluids and Structures, 2021 (100): 103173.
- T.Capurso, L. Bergamini, Torresi. “Design and CFD performance analysis of a novel impeller for double suction centrifugal pumps” [J]. Nuclear Engineering and Design, 2019 (341): 155-166.
- Thakkar S, Vala H, Patel V K, et al. “Performance improvement of the sanitary centrifugal pump through an integrated approach based on response surface methodology, multi-objective optimization and CFD” [J]. Journal of the Brazilian Society of Mechanical Sciences and Engineering, 2021, 43(1): 1-15.
- Wang Nengxiu, Liu Jafan. “Selection of impeller outlet parameters for centrifugal pumps” [J]. Journal of Huazhong University of Science and Technology, Natural Science Edition, 1987 (1): 97-102.
- Wang Wei, Shi Weidong, Jiang Xiaoping. “Optimal design of multistage centrifugal pump impeller based on orthogonal test and CFD” [J]. Journal of drainage and irrigation machinery engineering, 2016, 03: 1674-8530.
- Zhang Desheng, Zhang Qihua, Shi Weidong. “Numerical simulation fundamentals and applications of vane pump design” [M]. Beijing: Machinery Industry Press, 2015, 12.

NOMENCLATURE

φ the density of the fluid medium

η the efficiency

P the shaft power

ΔP the differential pressure between the pump inlet and outlet

H_T the theoretical head of the pump

μ_2 the vane outlet circumferential velocity

$v_{\mu 2}$ the vane outlet absolute velocity circumferential fractional velocity

μ_1 the blade inlet circumferential velocity (m/s)

$v_{\mu 1}$ the blade inlet absolute velocity circumferential fractional velocity

φ_2 is the impeller outlet discharge coefficient,

σ the Stodola slip coefficient

D_2 the outer diameter of the impeller (mm),

n the rotational speed

k the correction factor

ΔN_h the hydrodynamic power loss

ΔN_p the disc friction loss efficiency

k_1 the coefficient of velocity energy loss within the piezometric chamber

k_2 the dimensionless disc friction coefficient

R_2 the impeller outer edge radius

分布圖，驗證模型總體結構合理，但存在效率偏低、汽蝕嚴重的問題。設計正交試驗，以葉輪進口直徑，出口寬度，葉片出口角，葉片數作為實驗的四個因素，以效率和汽蝕為評價指標，分別得到兩組較好結構參數組合。建立了以襯塑泵效率損失和汽蝕余量最小的目標函數優化數學模型，以正交試驗兩組分析結果作為遺傳算法約束條件，對葉輪進口直徑、出口寬度，葉片出口角以及葉片數進行進壹步優化。結果顯示：當葉輪進口直徑為 100mm、出口寬度為 14mm，葉片出口角 27°、葉片數為 6 時，襯塑泵的效率提高了 2.36%，蒸汽體積分數降低了 0.151，效率、汽蝕都得到了明顯的改善。

基于遺傳算法的襯塑泵結構參數優化研究

方旭 王幼民 盧娜 柯啓迪 徐彬雪
安徽工程大學機械工程學院

摘要

效率低、汽蝕余量小壹直是低比速泵的難以解決的問題，其對襯塑泵影響更大。本研究以比轉速為 65 的襯塑泵為研究對象，用 PumpLinx 對襯塑泵內部流場進行模擬，得到了內部速度、壓力及流線